AIAA JOURNAL
Vol. 34, No. 9, September 1996

Effect of Inlet Reflections on Fan Noise Radiation

H. D. Meyer*
United Technologies Corporation, Windsor Locks, Connecticut 06096

The purpose of this initial investigation into the effect of inlet reflections on turbofan noise radiation is to discover whether the contribution from reflected waves is sufficient to warrant the extra complexity of including reflection in prediction methodologies. In making evaluations, two noise prediction codes have been used, the Ventres–Theobald–Mark (turbofan source noise generation) code (VTMC), and the Eversman radiation code (ERC), which predicts far-field acoustic radiation from a turbofan engine inlet. To first evaluate reflection, the ERC alone was used. Then a coupled code using both the ERC and a modified version of the VTMC that accepts reflected waves and generates updated stator loading was developed and used for exploratory runs. Results have shown that reflection from the inlet is significant in bands of frequencies about modal cutons. Reflected amplitudes are high enough to indicate that full coupling of the source and radiation fields is needed for accurate noise predictions.

I. Introduction

IT is known from the mathematics of duct acoustics that reflections will occur at points in a duct where there are changes in geometry. Therefore, when turbofan noise is generated, part of the energy from the source waves is reflected by the inlet back to the source region where it can influence the noise generation process. The purpose of the present work was to study reflection and its effect on fan noise radiation to see whether the contribution from reflected waves is sufficient to justify including this information in source noise prediction models.

This study was based on use of two noise prediction codes, the Ventres–Theobald–Mark (turbofan source noise generation) code (VTMC), and the Eversman radiation code (ERC), which predicts far-field acoustic radiation from a turbofan engine inlet. The programs treat the regions indicated in Fig. 1 (Ref. 1). The two regions are joined at an interface that we call the source input boundary. In the ERC, this interface is called the fan face, although the user may place this interface anywhere in the inlet.

Previous analysis by Topol[2] has considered the two regions in Fig. 1 with coupling of waves only from the source region to the radiation region. A complete match would require knowledge of the reflected waves at this surface. These reflected waves are the accumulated effect of reflection in the duct from the source input boundary to the inlet. Ignoring the reflections is justified if they are small. When reflections are large, a more sophisticated method might be preferable, one that would recognize waves passing the interface in both directions. This approach, called a coupled approach, could arrive at a solution, for example, by iterating between source and radiation analyses. Such an approach has been developed and used for work here by modifying the VTMC to accept reflected waves and generate updated stator loading.

The plots and tables presented here supercede those in Ref. 3 upon which this work is based. As part of more recent investigations of the coupling process, some cases run originally were rerun. The results of these runs were different than those obtained previously. The difference was caused by errors in the previous versions of both the ERC and the VTMC, which have since been corrected. Subsequently, all pertinent cases have been rerun. Based on reruns, the conclusions made in the original report are not affected by these differences.

Note that real fans have rotors that would be expected to attenuate the sound through rotor reflection and scattering. However, the rotor has been neglected because the purpose of the present work is to study the inlet/source coupling effect with a minimum of obscuring detail.

Finally note that wave propagation and reflection in ducts has been studied by numerous authors in the past (e.g., Refs. 4–8). This work has been mainly analytical, providing reflection coefficients, but not indicating the effect on the source. The present work obtains actual noise levels and is believed to be the first to address the effects of reflections on the source strength, i.e., blade loading.

II. Background

This section gives a brief sketch of the two codes that have been used in this work, the VTMC and the ERC. Details regarding the former can be found in Ventres et al.[9,10] Details for the latter are in Refs. 11–13. The regions treated by the VTMC and ERC are indicated in Fig. 1.

The VTMC is a Fortran program that calculates the sound produced by the interaction of stator vanes with the mean velocity deficit wakes generated by the rotor blades of a turbofan engine. The wakes produce unsteady loading on the vanes, and this loading then serves as the source for the sound. Some improvements were added to the code later; these are discussed in Philbrick and Topol[1] and Topol.[2] The fan/stator geometry for this study is shown in Fig. 2. The code predicts the amplitudes of both upstream and downstream propagating modes, along with their sound power, in an infinite annular duct. To accomplish this, it uses the standard Green's function approach.

In this approach, the Green's function is expressed as an expansion of normal duct modes; the loading (i.e., pressure distribution) exerted by the vanes on the fluid is evaluated for use in the Green's function integral that gives the pressure anywhere in the duct. Knowledge of the component of wake upwash velocity normal

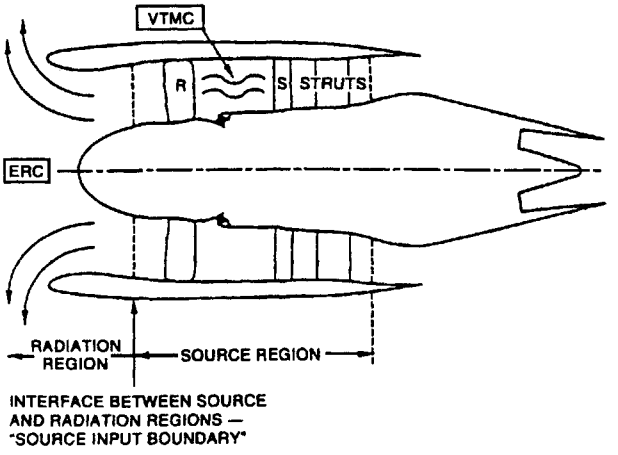

Fig. 1 Fan noise prediction system.[1]

Received April 12, 1994; revision received Dec. 21, 1995; accepted for publication Jan. 8, 1996.

*Senior Applied Mathematics Specialist, Hamilton Standard Division, MS 2M-FFGG18. Member AIAA.

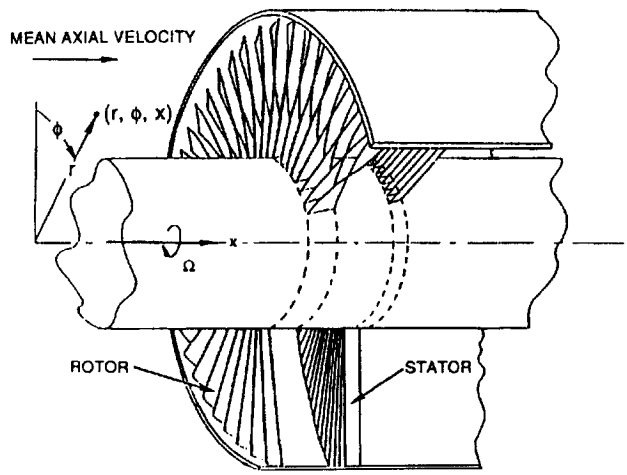

Fig. 2 Fan geometry used.[9]

to the surface of the stator vanes allows calculation of the pressure distribution on the vanes. This is done by dividing the stators into chordwise strips and computing the load on each strip, assuming the stators to be a linear cascade of flat plates. By means of this process, once the upwash is known, the upstream and downstream pressure mode amplitudes are obtained in straightforward fashion.

The ERC is a Fortran program used to study acoustic radiation from turbofan engines. It was developed under the direction of Walter Eversman.[12] The code uses standard and wave-envelope type finite elements and an underlying potential mean flow to predict noise from axisymmetric ducts with or without centerbodies. Solutions calculated within the code are in terms of the velocity potential, $\Phi_m(x, r)$, associated with circumferential mode m, where the complete solution is $\Phi = \Phi_m(x, r)\exp\{i(\omega t - m\phi)\}$. Here x is the axial coordinate, r and ϕ are polar coordinates, ω is rotor radian frequency, and t is time. Acoustic pressures are computed from Φ_m.

As input, both the index m and the reduced frequency (equivalently, rotor revolutions per minute or tip speed) must be set, along with complex forward propagating radial mode pressure amplitudes at the source input boundary. As mentioned in the previous section, the source input boundary is an arbitrary duct cross section where source information is input and is the interface between source and radiation regions (see Fig. 1). The ERC outputs complex backward propagating radial mode amplitudes at this same boundary. It also provides predictions for acoustic potential, pressure directivity, and acoustic pressure in the upstream radiation region.

III. Analytical Model for Coupled Code

To implement coupling, the VTMC was modified to accept reflected wave information from the ERC. As mentioned in the last section, the unmodified VTMC calculates the amplitudes p^W_{mns} of the pressure modes generated by the loading on the stator blades coming from the upwash w^W of the rotor wake. Here, m is the circumferential mode index, n the radial mode index, and s the harmonic of blade passage frequency. The preceding pressure amplitudes are those used to obtain the total acoustic pressure produced by the wake, which is given by the relation

$$p^W(x, r, \phi, t) = \sum_{s=-\infty}^{\infty}\sum_{n=1}^{\infty}\sum_{k=-\infty}^{\infty} p^W_{mns}\Psi_m(\kappa_{mn}r) \times \exp\{i(m\phi - \gamma_{mns}x - sB\Omega t)\} \quad (1)$$

In this expression, Ψ_m is the normal mode; t is time; κ_{mn} is the eigenvalue for mode (m, n); and γ_{mns} is the axial mode number given by

$$\gamma_{mns} = \frac{1}{1-M^2}\left[\frac{MsB\Omega}{c_0} \pm \sqrt{\left(\frac{sB\Omega}{c_0}\right)^2 - (1-M^2)\kappa^2_{mn}}\right] \quad (2)$$

where M is the inlet axial flow Mach number and c_0 is the speed of sound in the duct. In defining γ_{mns}, + or − is picked according to whether p^W_{mns} is for an upstream-going wave or for a downstream-going wave. Note that the circumferential mode index m must satisfy the condition that $m = sB - kV$ (see the discussion regarding this later in this section). This relation sets the value of m in Eq. (1) when summing over s and k. In Eq. (1) and for the rest of this section, refer to Fig. 2 regarding geometry and coordinates.

The modified VTMC computes an additional upwash w^R using the reflected wave information from the ERC and from this produces a reflected wave pressure amplitude coefficient p^R_{mns} that is added to the original. Thus the total upwash w on the stator is given by

$$w = w^W + w^R \quad (3)$$

and the total pressure amplitude p_{mns} by

$$p_{mns} = p^W_{mns} + p^R_{mns} \quad (4)$$

We start with an overview of the derivation of p^W_{mns}, which is the same for both the original and modified versions of the VTMC. Details will be brief, and so the reader is referred to the original VTMC documentation[10] for further description. Note that, at times, expressions here may vary slightly from expressions in Ref. 10. This is to provide correspondence with the actual code that was more recent than the documentation.

To obtain p^W_{mns}, one starts with the Green's function representation for pressure,

$$p(\boldsymbol{x}, t) = -\int_{-\infty}^{\infty}\int_S \boldsymbol{n}(\boldsymbol{y})\cdot\nabla G(\boldsymbol{x}, \boldsymbol{y}, t-\tau)\Delta p(\boldsymbol{y}, \tau)\,dS(\boldsymbol{y})\,d\tau \quad (5)$$

where S is the stator vane surface area, $\boldsymbol{x}$ and $\boldsymbol{y}$ are coordinate vectors (in cylindrical coordinates) in the duct, $\boldsymbol{n}$ is the unit normal to the stator blades, G is the Green's function, ∇ is the gradient operator, t and τ are time, and Δp is the pressure loading on the vanes. It then can be shown that the upwash has the form

$$w^W = \sum_s w_s \exp\left\{ik_s z + \frac{i2\pi vsB}{V} - isB\Omega t\right\} \quad (6)$$

relative to stator vane v, $v = 0, 1, \ldots, V-1$. In Eq. (6), B is the number of rotor blades, V the number of stator blades, Ω the rotor rotation rate, and s the same as before. The various w_s are the Fourier coefficients of the wake upwash at the sth harmonic of blade passage frequency, k_s is the chordwise wave number, and z is the local coordinate along each of the stator vanes.

Using the parameters in Eq. (6), an expression can be obtained for $\Delta\bar{p}_v$, which is the sth harmonic of the pressure loading Δp appearing in Eq. (5). It acts on vane v and is given by

$$\Delta\bar{p}_v = \rho_0 U_r w_s f_s(r, z)\exp\left\{\frac{-i2\pi vsB}{V}\right\} \quad (7)$$

where ρ_0 is the nominal fluid density, and U_r is the fluid velocity relative to the stator vanes. The quantity $f_s(r, z)$ is the elemental stator vane loading function that comes from solving

$$\exp\{ik_s z\} = \int_0^{2b} K_c(z-y)f_s(r, z)\frac{dy}{b} \quad (8)$$

where b is the vane semichord, and $K_c(z-y)$ is the Kernel function for a linear cascade and is discussed in Appendix B of Ref. 10.

Finally, by returning to Eq. (5), expanding G there in terms of eigenmodes, then using Eq. (7) and Fourier transform relations, one obtains the relation

$$\frac{p^W_{mns}}{\frac{1}{2}\rho_0 U^2} = \frac{\sigma_c(U_r/U)^2 V}{\pi(1-\sigma_r^2)\hat{k}_{mns}} \times \int_{\sigma_r}^1 \left(\frac{w_s}{U_r}\right)\Psi_m(X_{mn}\sigma)\left(\frac{m}{\sigma}\cos\alpha_s + \bar{\gamma}_{mns}\sin\alpha_s\right) \times \exp\left\{-i\left(\bar{\gamma}_{mns}\bar{\delta}_1 - \frac{m}{\sigma}\bar{\delta}_2\right)\sigma_c\right\}\tilde{b}C_{mns}(\sigma)\,d\sigma \quad (9)$$

for the amplitudes p^W_{mns} nondimensionalized by $\frac{1}{2}\rho_0 U^2$. In Eq. (9), U is the axial fluid velocity; $\sigma_c = 2b_T/r_D$ where b_T is the vane semichord at the tip and r_D is the duct outer radius; $\sigma_r = r_H/r_D$ where r_H is the hub radius; and $\bar{\gamma}_{mns} = \gamma_{mns} r_D$.

Further, in Eq. (9), $\hat{k}_{mns} = k_{mns} r_D$ where k_{mns} is the square root portion of γ_{mns}; $X_{mn} = \kappa_{mn} r_D$; $\sigma = r/r_D$; α_s is the stator stagger angle; $\bar{\delta}_1$ and $\bar{\delta}_2$ are nondimensionalized vane sweeps; $\bar{b} = b/b_T$ where b is the vane semichord; and the C_{mns} are the chordwise functions appearing in Ref. 10, but with minor modifications. Lastly, observe that the mathematics to obtain Eq. (9) imposes the condition that $m = sB - kV$, where k may be any integer.

For the modified version of the VTMC, the additional upwash w^R of Eq. (3) must be calculated using the reflected wave information provided by the ERC. Because each ERC run is for a fixed frequency, $\omega = sB\Omega$, w^R will not be given by a sum of terms over s as was w^W [see Eq. (6)] but will be given by only one such term. To obtain w^R, one starts with the velocity potential for the reflected wave, which is given by

$$\Phi^R_{ms} = \sum_{j=1}^{N} \Phi^-_{mjs} \Psi_m(\kappa_{mj} r) \exp\{i(-m\phi - \gamma^-_{mjs} x + sB\Omega t)\} \quad (10)$$

Each ERC run is made for a single choice of m and s. The coefficients Φ^-_{mjs} are the velocity potential complex modal amplitudes from the solution for the reflected waves. There are N of these, corresponding to the number of reflected radial modes, indexed by j, chosen for the ERC run. The number of upstream-going radial modes is the same. Equation (2), with the minus sign chosen, defines γ^-_{mns}. The modes can be cut on or cut off because both types are permitted by the ERC. The velocity v^R anywhere in the duct is calculated using $v^R = \nabla\Phi^R_{ms}(r, \phi, x)$. Then the component of v^R normal to the stator vanes is evaluated along the stator vanes to give

$$w^R = \sum_{j=1}^{N} w_{js} \exp\left\{ik_{js}z - i\frac{2\pi vsB}{V} - isB\Omega t\right\} \quad (11)$$

for the upwash, due to reflected waves, on vane v, $v = 0, 1, \ldots, V-1$. In Eq. (11), the various w_{js} are the Fourier coefficients of the reflection upwash at the sth harmonic of the blade passage frequency for radial mode j, and k_{js} is the chordwise wave number. The quantities w_{js} and k_{js} correspond to w_s and k_s in Eq. (6), but the expressions defining these are obviously very different. These quantities depend on $r, \alpha_s, \Phi^-_{mjs}, \gamma^-_{mjs}$, and the vane sweep parameters.

Proceeding now as previously for the wake case, one finally obtains the pressure modal amplitudes p^R_{mns} representing the effect of reflections from the inlet striking the stator and reradiating upstream. They are nondimensionalized by $\frac{1}{2}\rho_0 U^2$ and are given as follows:

$$\frac{p^R_{mns}}{\frac{1}{2}\rho_0 U^2} = \frac{\sigma_c (U_r/U)^2 V}{\pi(1-\sigma_r^2)\hat{k}_{mns}} \sum_{j=1}^{N} \int_{\sigma_r}^{1} \left(\frac{w_{js}}{U_r}\right) \Psi_m(X_{mn}\sigma)$$

$$\times \left(\frac{m}{\sigma}\cos\alpha_s + \bar{\gamma}_{mjs}\sin\alpha_s\right) \bar{b} C_{jmns}(\sigma)\, d\sigma \quad (12)$$

Just as for the wake case, the mathematics that gives Eq. (12) requires that m be such that $m = sB - kV$, where k may be any integer. The functions $C_{jms}(\sigma)$ depend on, among other things, the geometry, wave numbers, and the elemental vane chordwise pressure distributions, $f_{js}(r, z)$. Analogous to the situation for the $f_s(r, z)$ in the wake case, the $f_{js}(r, z)$ are calculated by solving the integral equation

$$\exp\{ik_{js}z\} = \int_0^{2b} K_c(z-y) f_{js}(r, z) \frac{dy}{b} \quad (13)$$

where $K_c(z-y)$ is the kernel function employed before. Note that the VTMC originally only computed cut-on modes. However, for work here, the code was extended to permit both cut-on and cut-off cases. Hence, the index n in Eq. (12) will take on values from 1 to N, so that pressure amplitudes may be for either cut-on or cut-off modes. Observe that there are no phase terms in Eq. (12) similar to the one in Eq. (9). This is because such terms have been absorbed into the w_{js} in Eq. (12).

IV. Code Validation

The ERC has been validated by means of numerous studies.[14–18] Of the work just cited, Ref. 14 is the most relevant with regard to work here because it verifies reflection coefficients against Cho's analytic results[8] for a hyperbolic horn and gives excellent agreement. Previous code errors (see Sec. I) were not present during these tests; the errors were introduced subsequently and were later removed. At any rate, the code has been reverified recently in efforts by Roy and Eversman in connection with work for Ref. 11. Also, there has been experimental validation by Topol and Philbrick.[1] The author has recently performed reflection coefficient comparisons for the same case as Astley.[14] As was the case for Astley, the agreement with Cho's solution was good.

The version of the VTMC used for this paper is the latest one and is one for which the previous errors mentioned in Sec. I have been eliminated. The author has thoroughly tested this version by making comparisons of pressure amplitudes from the VTMC for a very thin annulus test case vs results using Hanson's CUP2D two-dimensional turbofan aeroacoustics code.[19] Results from the two codes were virtually identical. Hanson's CUP2D code is an extension of the Smith code,[20] which is widely used in the aerospace community.

V. ERC Results

As a first evaluation of reflection, the ERC alone was used. The purpose of the runs was to determine whether reflection in these simple tests was large enough to justify proceeding further with more complicated coupled VTMC-ERC studies. From these runs, three types of results were obtained. The first were reflection ratio $|p^-/p^+|$ curves (see Figs. 3–5). The second were acoustic pressure contour plots, and the third were scattering ratios. The latter two items will be discussed later in this section. Note that reflection and scattering ratio results will be given for two separate setups, each involving a different inlet. These setups will be described later.

Regarding the reflection ratio curves, p^- and p^+ are the reflected and incident complex modal pressure amplitudes at the source input boundary. For each of the curves in Figs. 3–5, a unit modal amplitude was input for each choice of mode, (m, n), and runs were made over a range of engine tip speeds V_T. This unit mode input, for the nth radial mode, was our p^+, whereas p^-, which is the reflected wave amplitude for the nth radial mode, was obtained as output. Note that in Fig. 3 the dots indicated on the $(-6, 2)$ curve for tip speeds of 675 ft/s (206 m/s), 723 ft/s (220 m/s), and 900 ft/s (274 m/s) are there for later reference.

Runs for Fig. 3 were for the advanced ducted propeller (ADP) shown in Fig. 6. This geometry was also treated in Ref. 21. The setup treated a 16-blade, 22-vane, two-chord spacing, medium length ADP inlet model with duct radius of 8.63 in. (21.92 cm). The exterior Mach number was 0.2. The circumferential mode number studied was $m = -6$.

Figure 3 shows reflection ratios vs V_T for a fixed circumferential mode number of $m = -6$ and radial mode numbers of $n = 1$–3. Note that the peak of each curve occurs very close to the cut-on tip speed of the corresponding mode. Reflection was considered to be important in regions where reflection ratios were 0.5 or greater. The

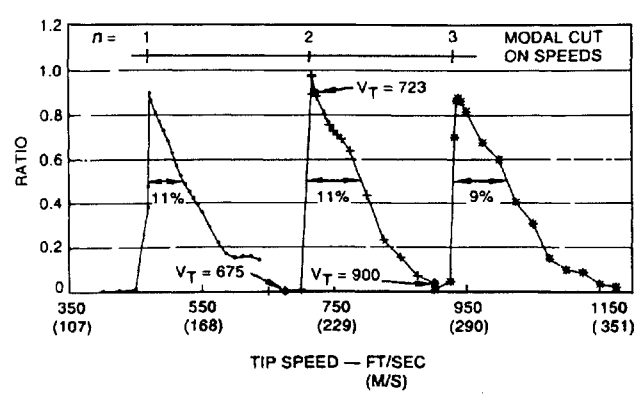

Fig. 3 Reflection ratios; $m = -6$ and $n = 1$–3; ADP model: •, mode (−6, 1); —+—, mode (−6, 2); and *, mode (−6, 3).

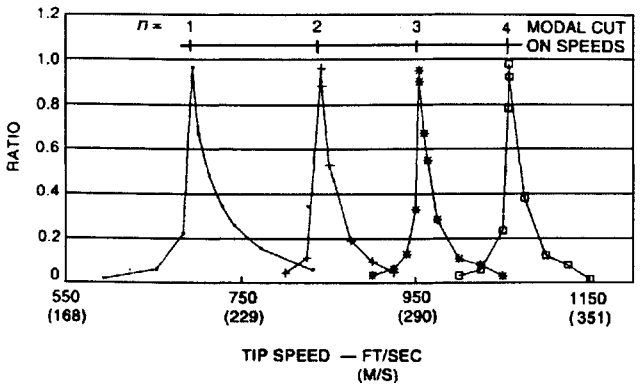

Fig. 4 Reflection ratios; m = 25 and n = 1–4; ERC model: •, mode (25, 1); —+—, mode (25, 2); *, mode (25, 3); and □, mode (25, 4).

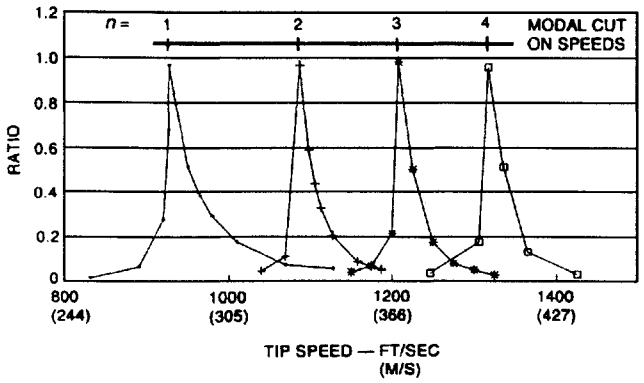

Fig. 5 Reflection ratios; m = 34 and n = 1–4; ERC model: •, mode (34, 1); —+—, mode (34, 2); *, mode (34, 3); and □, mode (34, 4).

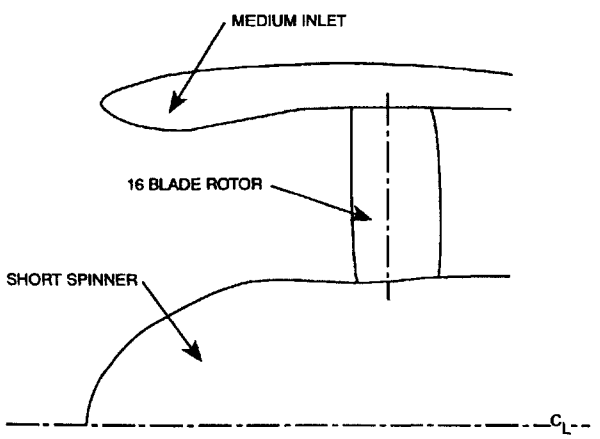

Fig. 6 Advanced ducted propeller inlet configuration.[21]

horizontal bands in Fig. 3 indicate these regions. To quantify the widths of these bands, a bandwidth W was defined as

$$W = \frac{\Delta V_T(\text{at}|p^-/p^+| = 0.5)}{(\text{midband } V_T)} \times 100\%$$

for each curve. In this expression, ΔV_T (at $|p^-/p^+| = 0.5$) is the change in V_T in passing from the left to the right side of the curves at a height of 0.5. As seen from Fig. 3, these bandwidths vary from 11 to 9%. It can be seen that these bands cover a considerable portion of the speed range evaluated.

Before the ADP model geometry was available, the same type of runs as for Fig. 3 were made for the fan inlet described by the ERC finite element mesh in Fig. 7. Dimensions shown are based on a unit fan tip radius. The model is for one of the test cases used in the past to test out ERC development and will be referred to as the ERC model. All results were for a Mach number M at the fan face of 0.5, a freestream Mach number of 0.3, and a 38-blade (B = 38) rotor. Curves for this setup are shown in Figs. 4 and 5. They illustrate behavior similar to that in Fig. 3. These curves, just as the previous ones, show that there is significant reflection in bands about cut on. Thus, Figs. 3–5 show that there can be considerable reflection across the range of tip speeds important to turbofan engines. Note that the peaks in Figs. 4 and 5 are sharper than those in Fig. 3. This seems to be because the cross section is more uniform for the ERC inlet. Because of this, cut on, where reflection is greatest, occurs in the rest of the duct at nearly the same tip speed as at the source input boundary. Thus reflections build up more sharply.

In the course of making the preceding $m = -6$ ERC runs for the ADP geometry, a number of contour plots showing rms acoustic pressure levels in the duct were generated. Three of these are presented here (see Figs. 8–10) to illustrate graphically that there are strong reflections in the duct at tip speeds where this would be expected. The three tip speeds are 675 ft/s (206 m/s), which occurs before second radial mode cut on; 723 ft/s (220 m/s), which falls just a bit after cut on; and 900 ft/s (274 m/s), which comes further after cut on. Cut on is at 717 ft/s (219 m/s). Refer to the (−6, 2) reflection ratio curve in Fig. 3 to see where these tip speeds are placed with respect to the peak. The first is to the left where the ratio is very small and reflection should be small. The second is to the right where the ratio is large and is typical of points in the range of tip speeds where much reflection would be expected. The third is farther to the right where the ratio starts to diminish and reflection should start to diminish. A unit second radial mode pressure amplitude was used as input at the source input boundary.

The contour plots show the reflection behavior found. The first contour plot, Fig. 8, for V_T = 675 ft/s (206 m/s), shows no reflection. The wave simply decays, as expected, for a cut-off mode. The next plot, Fig. 9, for V_T = 723 ft/s (220 m/s), shows significant reflection. The two sets of circles in the figure represent standing waves produced by forward- and backward-going (−6, 2) modes. This has been verified by comparing the wavelength measured from

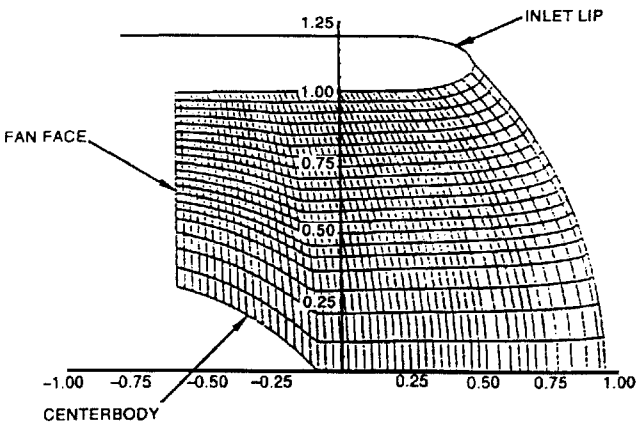

Fig. 7 Finite element model of ERC inlet.

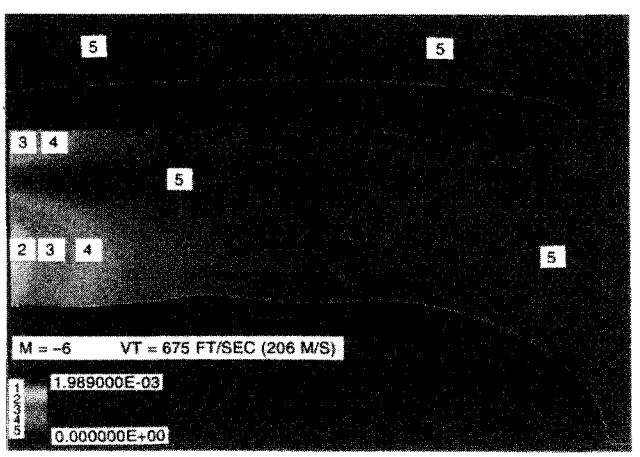

Fig. 8 Acoustic pressure contour plot for tip speed of 675 ft/s (206 m/s).

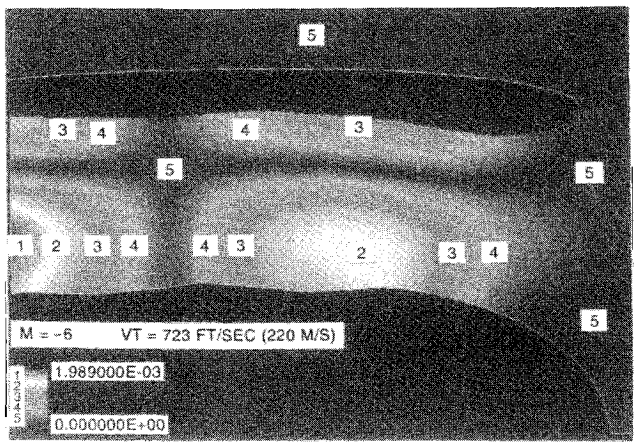

Fig. 9 Acoustic pressure contour plot for tip speed of 723 ft/s (220 m/s).

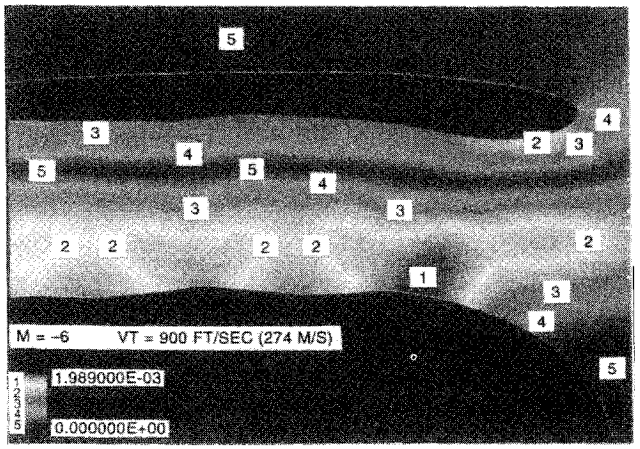

Fig. 10 Acoustic pressure contour plot for tip speed of 900 ft/s (274 m/s).

the plot with that predicted theoretically. The reflected wave amplitude must be similar to that of the outgoing wave to produce a standing wave pattern. The last plot, Fig. 10, for $V_T = 900$ ft/s (274 m/s), still shows standing waves and therefore reflections, but they are beginning to die out. The relative uniformity in the axial direction is indicative of propagation toward the inlet.

Returning now to Figs. 3–5, note that these deal only with reflection from a fixed radial mode n to n. There is also reflection from one radial mode to another. Since the ERC, as run here, provided reflected wave amplitudes for the first nine radial modes, not just for mode n, it was possible to construct Tables 1–3, which address the modal scattering issue. Data are from the same series of runs that produced Figs. 3–5. Table 1 is for the ADP case where $m = -6$, and Tables 2 and 3 are for the ERC inlet with $m = 34$. The entries in the tables are the ratios $|p^-/p^+|$, where p^- now represents the reflected pressure coefficient for each of the nine radial modes indicated. The inputs p^+ for Tables 1 and 2 are unit amplitudes for the relatively low order modes $(-6, 2)$ and $(34, 2)$. For Table 3, the input is a unit amplitude for a slightly higher order mode $(34, 4)$. As can be seen from the data, there is scattering into both higher- and lower-order modes relative to the input mode. From the data in the tables, it is seen that there can be considerable reflection from one radial mode into another.

Observe that a stairstep-type line has been added to each of the tables to indicate the division between modes that are cut on and cut off. Looking at ratios adjacent to these boundaries, note the tendency for the strongest reflected mode to move along these lines. This observation is based on only a small amount of data, and so it is something we would wish to look into further in the future.

Note that real aircraft nacelles include wall acoustic treatment that would attenuate modes of lower cut-off ratio. However, as seen here, scattering provides modes with higher cut-off ratios that would not be attenuated. These modes would be affected by the inlet internal reflection phenomenon investigated in this paper.

Table 1 Scattering ratios for unit input of mode $(-6, 2)$ into $(-6, n)$, ADP model

n \ V_T	675 (206)	700 (213)	723 (220)	775 (236)	825 (251)	900 (274)	925 (282)	950 (290)	ft/s (m/s)
1	0.004	0.009	0.016	0.064	0.018	0.024	0.015	0.022	
2	0.004	0.007	0.904	0.635	0.233	0.039	0.043	0.052	
3	0.004	0.004	0.005	0.010	0.011	0.037	0.173	0.339	
4	0.002	0.002	0.002	0.003	0.005	0.006	0.006	0.008	
5	0.001	0.001	0.001	0.001	0.002	0.002	0.002	0.003	
6	0.001	0.001	0.001	0.001	0.002	0.002	0.002	0.002	
7	0.000	0.000	0.000	0.000	0.001	0.001	0.001	0.001	
8	0.000	0.000	0.000	0.000	0.001	0.001	0.001	0.001	
9	0.000	0.000	0.000	0.000	0.000	0.000	0.000	0.000	

$n = 2$ cut on 717 ft/s (219 m/s)

$n = 3$ cut on 932 ft/s (284 m/s)

Table 2 Scattering ratios for unit input of mode $(34, 2)$ into $(34, n)$, ERC model

n \ V_T	1039 (317)	1069 (326)	1098 (334)	1106 (337)	1113 (339)	1128 (344)	1187 (362)	1247 (380)	ft/s (m/s)
1	0.022	0.028	0.064	0.073	0.073	0.069	0.047	0.048	
2	0.044	0.110	0.590	0.439	0.329	0.203	0.050	0.009	
3	0.005	0.006	0.011	0.012	0.012	0.013	0.054	0.095	
4	0.000	0.000	0.001	0.001	0.001	0.002	0.004	0.008	
5	0.000	0.000	0.000	0.000	0.000	0.000	0.001	0.001	
6	0.000	0.000	0.000	0.000	0.000	0.000	0.000	0.000	
7	0.000	0.000	0.000	0.000	0.000	0.000	0.000	0.000	
8	0.000	0.000	0.000	0.000	0.000	0.000	0.000	0.000	
9	0.000	0.000	0.000	0.000	0.000	0.000	0.000	0.000	

$n = 2$ cut on 1088 ft/s (332 m/s)

$n = 3$ cut on 1208 ft/s (368 m/s)

Table 3 Scattering ratios for unit input of mode $(34, 4)$ into $(34, n)$, ERC model

n \ V_T	1187 (362)	1247 (380)	1306 (398)	1336 (407)	1365 (416)	1425 (434)	ft/s (m/s)
1	0.003	0.002	0.008	0.031	0.026	0.018	
2	0.004	0.003	0.007	0.019	0.014	0.023	
3	0.034	0.054	0.019	0.027	0.024	0.022	
4	0.017	0.033	0.173	0.509	0.127	0.028	
5	0.009	0.013	0.019	0.052	0.052	0.295	
6	0.001	0.001	0.002	0.004	0.005	0.016	
7	0.000	0.000	0.000	0.000	0.000	0.001	
8	0.000	0.000	0.000	0.000	0.000	0.000	
9	0.000	0.000	0.000	0.000	0.000	0.000	

$n = 3$ cut on 1208 ft/s (368 m/s)

$n = 4$ cut on 1318 ft/s (402 m/s)

$n = 5$ cut on 1420 ft/s (433 m/s)

VI. Coupled Run Results

The information presented in the preceding section showed there is considerable reflection activity in the duct. These results justified proceeding further to investigate reflections using the coupled VTMC-ERC setup discussed in Sec. III. To this end, a series of exploratory computer runs was made to show the effect on both source and far-field regions of feeding back reflections. For a given tip speed, each run involved first executing the VTMC and then feeding its output as input to an initial ERC run. Reflected wave output from this ERC run, at the source input boundary, was next fed into a second VTMC run where it provided updated stator blade loading. The resulting VTMC output was then used as input for a second ERC run.

These tests were made for the same ADP geometry as described earlier in Sec. V. They covered a tip speed range of 650–900 ft/s (198–274 m/s). Figures 11 and 12 show results for this range that

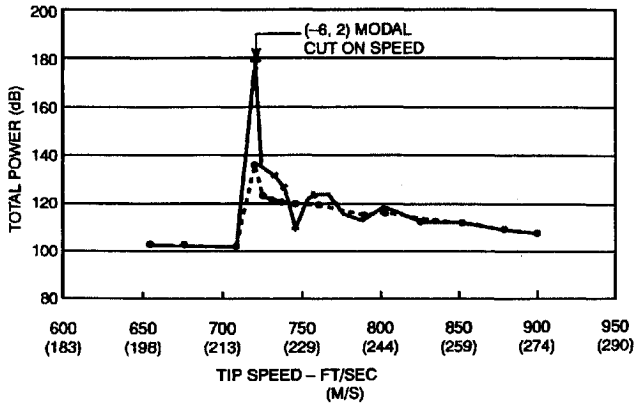

Fig. 11 Comparison of VTMC runs. Total upstream power for $m = -6$: •, base run and —+—, coupled.

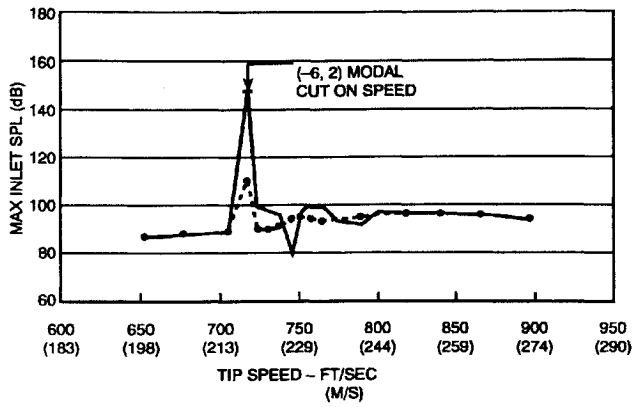

Fig. 12 Comparison of ERC runs. Sound pressure level at 10 inlet radii for $m = -6$: •, base run and —+—, coupled.

includes second radial mode cut on. The exterior Mach number was 0.2. As before, the circumferential mode number studied was $m = -6$. In the coupled VTMC runs, the first nine radial modes for $m = -6$, not all of which were cut on, were used.

Figure 11 compares total upstream sound power in the first and second VTMC runs, i.e., before and after coupling, as a function of tip speed. Note that cut on for the second radial mode, $(-6, 2)$, is at 717 ft/s (219 m/s), where the two curves peak. Below second mode cut on, only radial mode $(-6, 1)$ contributes to power; above this point both modes $(-6, 1)$ and $(-6, 2)$ contribute. In a band of tip speeds above second radial mode cut on, there is a sizable increase in total power from the uncoupled to the coupled case. [Note that the increase just below cut on of the $(-6, 2)$ mode, in both Figs. 11 and 12, should be disregarded; we trust that, if additional points were computed in this vicinity, then there would be virtually no delta.] At a typical point $V_T = 738$ ft/s (225 m/s), a bit removed from cut on, in Fig. 11, the increase is 5.9 dB.

Figure 12 shows a similar comparison for the ERC between the first and second runs, where the first is before coupling and the second is after. The ordinate here is maximum sound pressure level (SPL) at 10 inlet radii, rather than total power as before. This quantity is used because it, rather than total power, is easily derivable from ERC runs. Also, this parameter gave a good indication as to whether reflection was having an effect. Just as for the prior VTMC cases, plots in Fig. 12 show a band above cut on where the change in noise levels due to reflection is significant, and at $V_T = 738$ ft/s (225 m/s), the increase in SPL was slightly less than the power increase computed via the VTMC.

Results are for one iteration step and show that reflection is important. Study of converged results is also planned.

VII. Concluding Remarks

In this paper, reflection and its effect on turbofan noise radiation were studied to see whether the contribution from reflected waves was sufficient to warrant the extra complexity of feeding predictions back from a radiation model to a source model. The VTMC and ERC were employed in this effort.

Using the ERC alone, unit amplitude forward propagating modes were input at the source input boundary. The code computed the reflected amplitudes for the same radial modes as those input. The ratio of these amplitudes, $|p^-/p^+|$, vs rotor tip speed, for a selection of circumferential mode and radial mode pairs (m, n), indicates that in significantly wide bands about cut-on tip speed there is significant reflection from the inlet. There was also significant reflection into other radial modes in the vicinity of cut-on boundaries. Contour plots were derived for the ADP inlet and $m = -6$ in the vicinity of second radial mode cut on. The presence of standing waves for a tip speed just a bit above second radial mode cut on indicated substantial reflections.

A method of coupling the VTMC source and the ERC radiation models that recognizes waves crossing the interface in both directions was developed. Computer runs were made using this coupled approach for an ADP model, with circumferential mode order $m = -6$. For this process, a first VTMC run was made. Output from this first run was fed into the ERC. Then this VTMC-ERC cycle was repeated. Plots of total sound power vs tip speed for propagating waves in the duct and of maximum sound pressure level vs tip speed for waves at 10 inlet radii in the far field showed significant differences in radiation levels in a band above the second radial mode cut on. For instance, at a tip speed of 738 ft/s (225 m/s), the increase in total power in the duct was 5.9 dB; a similar increase in SPL was also seen in the far field. Cut on was at 717 ft/s (219 m/s).

Based on the preceding results, we can conclude that coupling reflection back to the source does have an effect on net radiation and should be included in predictions. Work here has been for one iteration step. In the future, converged results will also be studied.

Acknowledgments

This work was supported by Pratt and Whitney with funding from NASA Lewis Contract NAS3-25952. Dennis Huff was NASA Lewis contract manager. The author would like to thank Donald B. Hanson of Pratt and Whitney for suggesting the project treated here and for his support and helpful suggestions. Appreciation also should go to David A. Topol, who introduced the author to his acoustic pressure contour plotting setup at Pratt and Whitney and assisted him in its use and in interpretation of the plots. Finally, thanks should go to the reviewers for their useful comments. Regarding the computer codes used in this effort, the VTMC was developed originally by Bolt, Beranek, and Newman for NASA Lewis; later improvements were added by Pratt and Whitney. The ERC was developed at the University of Missouri–Rolla.

References

[1]Philbrick, D., and Topol, D., "Development of a Fan Noise Design System, Part 1: System Design and Source Modeling," AIAA Paper 93-4415, Oct. 1993.

[2]Topol, D., "Development of a Fan Noise Design System, Part 2: Far-Field Radiation and System Evaluation," AIAA Paper 93-4416, Oct. 1993.

[3]Meyer, H. D., "Fan Noise Prediction System Development: Source/Radiation Field Coupling and Workstation Conversion for the Acoustic Radiation Code," Hamilton Standard Div., United Technologies Corp., HSER-16304, Windsor Locks, CT, April 1994.

[4]Levine, H., and Schwinger, J., "On the Radiation of Sound from an Unflanged Circular Pipe," *Physical Review*, Vol. 73, Feb. 1948, pp. 383–406.

[5]Rice, E. J., "Multimodal Far-Field Acoustic Radiation Pattern Using Mode Cutoff Ratio," *AIAA Journal*, Vol. 16, No. 9, 1978, pp. 906–911.

[6]Morfey, C. L., "Rotating Pressure Patterns in Ducts: Their Generation and Transmission," *Journal of Sound and Vibration*, Vol. 1, Jan. 1964, pp. 60–87.

[7]Zorumski, W. E., "Generalized Radiation Impedances and Reflection Coefficients of Circular and Annular Ducts," *Journal of the Acoustical Society of America*, Vol. 54, Dec. 1973, pp. 1667–1673.

[8]Cho, Y. C., "Sound Radiation from Hyperboloidal Inlet Ducts," AIAA Paper 79-0677, March 1979.

[9]Ventres, C. S., Theobald, M. A., and Mark, W. D., "Turbofan Noise Generation, Volume 1: Analysis," NASA CR 167951, July 1982.

[10]Ventres, C. S., Theobald, M. A., and Mark, W. D., "Turbofan Noise Generation, Volume 2: Computer Programs," NASA CR 167952, July 1982.

[11]Roy, I. D., and Eversman, W., "Improved Finite Element Modeling of the Turbofan Engine Inlet Radiation Problem," American Society of Mechanical Engineers, ASME Paper 93-WA/NCA-13, New York, Nov. 1993.

[12]Eversman, W., Parrett, A. V., Preisser, J. S., and Silcox, R. J., "Contributions to the Finite Element Solution of the Fan Noise Radiation Problem," *Transactions of the American Society of Mechanical Engineers*, Vol. 107, April 1985, pp. 216–223.

[13]Parrett, A. V., and Eversman, W., "Wave Envelope and Finite Element Approximations for Turbofan Noise Radiation in Flight," *AIAA Journal*, Vol. 24, No. 5, 1986, pp. 753–760.

[14]Astley, R. J., "Wave Envelope and Infinite Elements for Acoustical Radiation," *International Journal for Numerical Methods in Fluids*, Vol. 3, Sept.–Oct. 1983, pp. 507–526.

[15]Astley, R. J., "Acoustical Radiation in Moving Flows: A Finite Element Approach," *Proceedings of the 1983 International Conference on Computational Techniques and Applications* (Sydney, Australia), North-Holland, Amsterdam, 1984, pp. 685–698.

[16]Silcox, R. J., "Experimental Investigation of Geometry and Flow Effects on the Acoustic Radiation from Duct Inlets," AIAA Paper 83-0713, April 1983.

[17]Preisser, J. S., Silcox, R. J., Eversman, W., and Parrett, A. V., "A Flight Study of Tone Radiation Patterns Generated by Inlet Rods in a Small Turbofan Engine," AIAA Paper 84-0499, Jan. 1984.

[18]Baumeister, K. J., "Utilizing Numerical Techniques in Turbofan Inlet Acoustic Suppressor Design," NASA TM 82994, Oct. 1982.

[19]Hanson, D. B., "Coupled 2-Dimensional Cascade Theory for Noise and Unsteady Aerodynamics of Blade Row Interaction in Turbofans, Volume 2—Documentation for Computer Code CUP2D," NASA CR 4506, Jan. 1994.

[20]Smith, S. N., "Discrete Frequency Sound Generation in Axial Flow Turbomachines," Aeronautical Research Council, London, Report R. & M. 3709, March 1972.

[21]Woodward, R. P., Bock, L. A., Heidelberg, L. J., and Hall, D. G., "Far-Field Noise and Internal Modes from a Ducted Propeller at Simulated Aircraft Takeoff Conditions," AIAA Paper 92-0371, Jan. 1992.